Temperature Dependent Surface Electrochemistry on Pt Single Crystals in Alkaline Electrolyte: Part 3: The Oxygen Reduction Reaction

T.J. Schmidt[1*], V. Stamenkovic, P.N. Ross, Jr., N.M. Markovic[*]

Materials Sciences Division, Lawrence Berkeley National Laboratory, University of California, Berkeley, CA 94720, USA

Abstract

The kinetics of the oxygen reduction reaction (ORR) was studied in alkaline electrolyte at 293-333K on Pt(hkl) surfaces by means of the rotating ring-disk electrode technique with solution phase peroxide detected at the ring electrode. The ORR on Pt(hkl) was found to be highly structure sensitive with activities increasing in the sequence (111) > (100) > (110)(1x2). Very similar apparent activation energies (37-45 ± 5 kJmol^{-1}, η = 0.35 V) were found on all three surfaces. Furthermore, at elevated temperature, significantly smaller amounts of peroxide are formed in agreement with enhanced peroxide reduction rates by increasing temperature. We found that the Tafel slopes on all three single crystal surfaces decrease with increasing temperature, indicating that the logi-E relationship is not represented by a classical Butler-Volmer expression. Based on the kinetic analysis of the polarization curves and from simulations of logi-E curves, we propose that the rate of the ORR on Pt(hkl) in alkaline solution is mainly determined by the potential/temperature dependent surface coverage by OH_{ad}. We propose two modes of action of the OH_{ad}: *i)* OH_{ad} blocks the adsorption of O_2 on active platinum sites; and *ii)* OH_{ad} alters the adsorption energy of intermediates which are formed during the ORR on Pt sites.

---

[*] Corresponding Authors, tom.schmidt@psi.ch and nmmarkovic@lbl.gov

[1]present address: Paul-Scherrer-Institute, Laboratory of Electrochemistry, CH-5232 Villigen-PSI, Switzerland

1. Introduction

The oxygen reduction reaction (ORR) is one of the key reactions in electrochemical energy conversion and storage devices like fuel cells [1-3] and batteries [4,5]. Most of the earlier studies were carried out on polycrystalline electrodes of either pure metals or poorly characterized alloy surfaces. Recently, however, considerable effort has been directed to the study of the ORR on single crystal electrodes [6-9] and on well-characterized bimetallic surfaces [9-12]. Of various systems examined, in the past few years extensive studies have been undertaken with platinum single crystal surfaces in order to establish the influence of the surface structure on the ORR kinetics. These studies unambiguously showed that the ORR on Pt(hkl) is a structure sensitive reaction, which in aqueous electrolytes arises mainly from the structural sensitivity of the adsorption of spectator species like anions from the supporting electrolyte [8,9,13,14]. In contrast to acidic solution, the ORR studies on well defined Pt single crystals in alkaline electrolyte is scarce. Even though alkaline electrolyte may be of less interest technologically, research in alkaline electrolyte can give insights into the ORR chemistry due to the absence of specific adsorption of spectator anions in supporting electrolyte [2,8,9,15-17].

The present study is the third and final part on the catalytic properties of Pt(hkl) surfaces in alkaline solution, the two previous being the temperature dependent kinetics of CO oxidation [18] and the hydrogen evolution/oxidation reaction (HER/HOR) [19]. The ORR was studied over a temperature range between 293 K and 333 K in 0.1 M KOH. We first present a detailed analysis of the kinetic parameters for the ORR, *e.g.*, Tafel slopes, and activation energies, and then discuss the reaction pathway by which O_2 is reduced on Pt(hkl) in alkaline solution.

2. Experimental

The pretreatment and assembly of the Pt(hkl) single crystals (0.283cm^2) in a RRDE configuration was fully described previously [13,18]. In short, following flame annealing in a hydrogen flame and cooling in a mild stream of Ar, the single crystal was mounted into the disk position of an insertable ring disk electrode assembly (*Pine Instruments*). Subsequently, the electrode was transferred into a thermostated standard three compartment electrochemical cell and immersed into the Ar-purged/O_2-purged electrolyte (Ar: *Bay Gas Research Purity*; 0.1 M KOH: *Aldrich Semiconductor Grade* prepared with triply pyrodistilled water) under potentiostatic control at ≈ 0.1 V. In order to avoid both surface contamination with impurities present in even the most meticulously prepared alkaline electrolytes as well as the potential induced disordering of Pt(hkl) surfaces at higher positive potentials, for each temperature electrodes were re-annealed and transferred into freshly prepared electrolytes. Furthermore, to minimize surface contamination, polarization curves at 400-2500 rpm were recorded immediately following a first blank potential sweep between 0.05 and 0.9 V. It is noteworthy that to minimize surface disordering by irreversible oxide formation, the positive potential limit was restricted to ca. 0.9 V, except for the last anodic sweep (2500 rpm) in which the anodic potential was extended up to 1.05 V. The last polarization curve was used to establish the temperature effect on the Tafel slopes.

A circulating constant temperature bath (*Fischer Isotemp Circulator*) maintained the temperature of the electrolyte within ± 0.5 K. All measurements were conducted non-isothermally, *i.e.*, keeping the temperature of the reference electrode constant (≈ 298 K) while that of the working electrode was varied from 293 K to 333 K. The reference electrode was a

saturated calomel electrode (*SCE*) separated by a closed electrolyte bridge from the working electrode compartment in order to avoid chloride contamination. All potentials, however, refer to that of the reversible hydrogen electrode in the same electrolyte, calibrated from the reversible potential for the HOR/HER obtained during our measurements [19]. Oxygen was supplied from *Bay Gas* (*Research Purity*). The polycrystalline Pt ring electrode for detection of HO_2^- was potentiostated at 1.2 V *vs*. RHE. The collection efficiency of the RRDE setup was N = 0.22 ± 5 %. The measurements on Pt(110) were carried out on the reconstructed surface with (1x2) geometry, prepared according to ref. [20], hereafter this surface is denoted as Pt(110) only. The reconstructed (1x2) surface was previously found to be stable in the potential range applied in the present study [20].

3. Results

3.1 Review of Cyclic Voltammetry on Pt(hkl) in 0.1 M KOH

The base voltammetries of Pt(111), Pt(100), and Pt(110) in 0.1 M KOH at 293 K and 333 K are summarized in figures 1a-3a, respectively. Since the interpretation of the temperature dependent base CV's of Pt(hkl) in alkaline electrolyte has been described in part 1 of these studies in detail [18], we review only briefly that interpretation here for completeness. Figure 1 shows that Pt(111) is the only surface which exhibits three separate potential regions: the hydrogen underpotential deposition region (H_{upd}, $0 < E < 0.4$ V) is directly followed by the double layer region (ca. $0.4 \text{ V} < E < 0.6$ V) and then the so-called 'butterfly region' ($0.6 < E < 0.9$ V). The "butterfly" feature in alkaline solution is commonly assumed to represent the discharge of OH^- to form OH_{ad} [21]. In contrast to this highly reversible state of adsorbed OH, a more irreversible 'oxide' state is formed at potentials above

0.9 V. It is noteworthy, however, that the chemical state of this irreversible form of oxide is still unknown. As already mentioned in our detailed study on temperature effects on the base CV of Pt(111) in acid and alkaline electrolyte [17], the oxide peak at ca. 1.1 V (293 K) is shifting to more negative potentials with increasing temperature. Additionally, the concomitant oxide reduction peak in the cathodic sweep direction is shifting to more positive potentials at higher temperatures, fig. 1a. This implies that this oxidation process is becoming more reversible with increasing temperature. In contrast, the formation of both the reversible OH_{ad} and H_{upd} ad-layers are not affected significantly by temperature changes [17,18]. Details about the thermodynamics and energetics of H_{upd} and OH_{ad} on Pt(111) in alkaline solution can be found in ref. [17]. Fig.2a and 3a show that a true double-layer potential region does not exist on either Pt(100) (figure 2a) or on Pt(110) (figure 3a), and that the H_{upd} region overlaps with the OH_{ad} formation [18]. In fact, we recently demonstrated by titrating Pt(hkl) surfaces with the continuous oxidation of CO that some OH_{ad} is co-adsorbed with H_{upd} even at potentials below ca. 0.1 V, since even at these low potentials significant CO oxidation currents could be observed. A further inspection of cyclic voltammograms clearly show that the initial reversible formation of OH_{ad} on both Pt(100) and Pt(110) (up to ca. 0.7 V), is followed by a more irreversible formation of what we call the "oxide" [18]. At this point it is important to note that the tendency to become (irreversibly) oxidized, especially at elevated temperatures, increased in the sequence Pt(111) < Pt(100) < Pt(110) [18,19]. As we will demonstrate below, it turns out that the order of oxophilicity of Pt single crystal surfaces plays a dominant role in the kinetics of the ORR on Pt(hkl) in alkaline solution.

3.2 Potentiodynamic ORR on Pt(hkl) in KOH

The families of polarization curves for the ORR on Pt(111), Pt(100), and Pt(110) at 333 K (50 mVs^{-1}) are illustrated in figure 1b, 2b, 3b, respectively. Although the same data sets were recorded at 293 K and 313 K, these results are not shown in this work; for details we refer to our previous papers [12,14]. A close inspection of figures 1b-3b reveals that the region of mixed kinetic-diffusion control (0.75 V < E < 1 V) is followed by diffusion limited current densities below ca. 0.7 V. At E < 0.4 V, *i.e.*, in the H_{upd} region, a deviation of the diffusion limited currents to lower values can be observed. This deviation can be quantitatively related to the formation of HO_2^- as demonstrated by the HO_2^- detection on the ring electrode [8,12,14]. The corresponding ring currents obtained at 293 K, 313 K, and 333 K in figure 1-3 are directly converted into the current efficiency for HO_2^-, $x_{HO_2^-}$,according to eq. 1 [22,23].

$$x_{HO_2^-}[\%] = 100 \cdot \frac{2 \cdot I_R / N}{I_D + I_R / N} \qquad \text{Eq. 1}$$

In this equation, I_D and I_R are the disk and ring currents, respectively, with N being the collection efficiency. Figures 1-3 clearly demonstrate that the decrease of the diffusion limited current densities in the H_{upd} region is directly accompanied by the enhanced formation of peroxide (on Pt(111) up to ca. 23 % at 293 K). At lower overpotentials, *i.e.*, in the mixed kinetic-diffusion region, almost no peroxide can be observed (< 1 %) on either of the Pt surfaces. It is noteworthy that the current efficiency for peroxide is decreasing with increasing temperature by roughly a factor of two at the lower potential limit. Given that the surface coverage by OH_{ad} is only slightly affected by the temperature at these electrode potentials, it

is reasonable to conclude that the rate of peroxide reduction at higher temperatures is enhanced throughout the temperature activation of O-O bond breaking in the HO_2^- ion.

In order to assess the true kinetics of the ORR on Pt(111) in KOH, the logi/E-relationships (Tafel plots) at 293 K, 313 K, and 333 K are plotted in figure 1d-3d. The ORR on Pt(hkl) seems to be an highly activated process due to the observed increase of the reaction rates with increasing temperature. The apparent activation energy, $\Delta H^{\neq}$, was evaluated in an Arrhenius-analysis, see figure 4, at a constant overpotential, η, of $\eta = 0.35$ V according to a procedure described elsewhere [23,24] resulting in a value of 47, 42, and 37 $kJmol^{-1}$ on Pt(111), Pt(100), and Pt(110), respectively (table 1). Similar values around ca. 40 $kJmol^{-1}$ were previously found in 0.05 M H_2SO_4 extrapolated at the reversible potential [25]. The logi/E-relationships at the different temperatures can be fitted by straight lines in order to determine the Tafel slopes. On all Pt(hkl) surfaces we find that Tafel slopes are decreasing with increasing temperatures (table 1), which is at variance with the results obtained in sulfuric acid solution [25]. Values for Pt(111) and Pt(100) are between 86 and 57 $mVdec^{-1}$ and 112 and 60 $mVdec^{-1}$, respectively. On Pt(110), the slopes are slightly higher going from ca. 192 to 83 $mVdec^{-1}$.

Comparison of activities of the ORR on Pt(hkl) surfaces in the potential region where the reaction is under kinetic control shows that the kinetics increase in the order P(110)(1x2) < Pt(100) < Pt(111). Notice that in a previous study at room temperature [14], we found the least active surface was Pt(100). This discrepancy can be attributed to two factors: *i)* the prehistory of electrodes in the present work, *e.g.* the number of cycles into the OH_{ad}-/oxide-region, as well as the positive potential limits were slightly different from that

used in reference [14]; *ii)* in the present study we carefully prepared the reconstructed Pt(110)(1x2) surface *vs*. the (1x1) surface in [14].

In the experimental section, we emphasized that due to a possible contamination of Pt single crystals by impurities present in alkaline solutions, a rather fast sweep rate was used to record the polarization curves for the ORR. To establish the steady-state i *vs*. E relationship, the electrode potential was held for 5 min in the potential region where the ORR is under mixed kinetic-diffusion control. A representative example is shown in figure 6 for the Pt(111) surface. In order to minimize a possible contamination problem enhanced by a continuous rotation, we chose not to rotate the electrode while the potential was held in the potential region designated on figure 6. To find the "steady-state' activity, after a 5 min. hold at the fixed potential with a stationary electrode, rotation was applied and after 5 s the current was recorded at 1600 rpm, see circles in figure 6. The resulting current is very similar to that recorded under the fast sweep rate, confirming that for the oxygen reduction reaction on clean Pt surfaces the applied sweep rate of 50 mV provides reliable steady-state activity.

4. Discussion

Of various reaction schemes proposed for the ORR [2,4,16,26], one suggested, *e.g.*, in ref. [9,27,28] appears to be the most effective to describe the reaction pathway by which O_2 is reduced at the Pt-liquid interface:

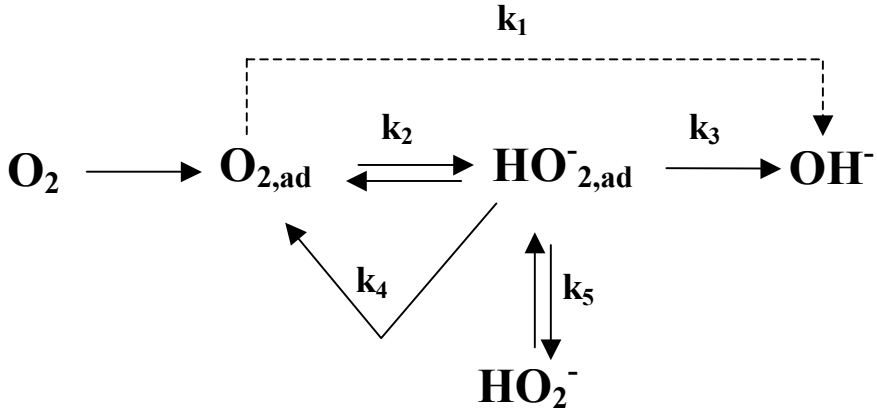

Based on this scheme, adsorbed O_2 on the disk electrode can react either directly to OH^- (k_1 path, 4 e^- reduction) or follows a serial pathway through the intermediate formation of adsorbed HO_2^- (k_2 path, 2e^- reduction), which, in a second step, can be further reduced to OH^- (k_3, 2 + 2 e^- reduction). Produced $HO_{2,ad}^-$ molecules can also desorb from the disk electrode to the solution phase (k_5 path). Additionally, $HO_{2,ad}^-$ can be chemically decomposed to form water and O_2 in a heterogeneously catalyzed reaction step (k_4 path). Although a number of important problems pertaining to the interpretation of the reaction pathway for the ORR on Pt(hkl) have yet to be resolved, recent studies from our laboratory [8,9] suggest that the serial reaction pathway through the formation of $HO_{2,ad}^-$ (with k_1 being essentially zero), may be operative on all Pt single crystal surfaces. We note that depending on the availability of bare (no OH_{ad} or H_{ad}) Pt sites peroxide may ($k_5 > k_3$) or may not ($k_3 >> k_5$) be observed on the ring electrode [9]. In ring-disk measurements, the solution phase intermediate HO_2^- desorbing from the electrode surface can be detected on the independently polarized Pt ring (E_{ring} = 1.2 V *vs.* RHE) electrode by oxidizing it back to O_2. Accepting that the "serial' reaction pathway is operative on Pt(hkl) surfaces, possible elementary steps involving different reaction intermediates can be given as the following: .

$$O_2 \Rightarrow O_{2,ad} \quad (1)$$

$$O_{2,ad} + 1\,e^- \Rightarrow O_{2,ad}^- \quad (1a)$$

$$O_{2,ad}^- + H_2O \Rightarrow HO_{2,ad}^- + OH_{ad} \quad (1b)$$

$$HO_{2,ad}^- = HO_2^- \quad (2)$$

$$HO_{2,ad}^- = O_{ad} + OH_{ad} \quad (3a)$$

$$O_{ad} + H_2O + 1\,e^- \Rightarrow OH_{ad} + 2\,OH^- \quad (3b)$$

$$OH_{ad} + 1\,e^- = OH^- \text{ (x2)} \quad (4)$$

For Pt surfaces, steps (1a) and (1b) are generally considered to be rate determining [9,15,29], and are often written as a single reaction in which $(O_2^-)_{ad}$ does not appear explicitly. Likewise (3a) and (3b) are often combined to yield a single 1 e^- step in which O_{ad} does not appear explicitly. In order to explicitly refer only to elementary reactions, we prefer the notation above. With (1a) and (1b) rate determining, steps (2) – (4) are at equilibrium. At all potentials the coverage by OH_{ad} on Pt(hkl) is unchanged by the presence of O_2, *i.e.,* the coverage is determined entirely by the equilibrium constant of step (4). This implies that the equilibria for steps (3a,b) and (4) are shifted strongly to the right hand side, and that the coverage by $(HO_2^-)_{ad}$ in particular is low, as is the amount of HO_2^- in solution. The mechanism is very useful in establishing the role of OH_{ad} in the structure sensitivity of the reaction on Pt(hkl). Stronger adsorption of OH_{ad} causes the rate of (1a and 1b) to "back up" due to the accumulation of OH_{ad} on the surface, blocking sites for electron transfer to O_2. Very recently, closely following Tarasevich's analysis for the ORR on polycrystalline electrodes [2], we proposed a general rate expression of the ORR on Pt(hkl) in which the kinetics is determined either by the free Pt sites available for the adsorption of O_2 and/or by

the change of Gibbs energy of adsorption of reaction intermediates. Assuming *i)* that the addition of the first electron to O_2 is the rate determining step and *ii)* that reactive intermediates in Eqs. 1-4 are adsorbed with low coverage (at least compared to the surface coverage by hydroxyl species), the rate expression is then [30]

$$i = nFKc_{O2} \cdot (1 - y\Theta_{OH})^x \cdot \exp\left(\frac{-\alpha FE}{RT}\right) \cdot \exp\left(\frac{-\gamma r_{OH}\Theta_{OH}}{RT}\right) \quad \text{Eq. 5}$$

with Θ_{OH} being the potential dependent coverage of OH_{ad}, x is the order of active sites (either one or two), y = 1 is the number of Pt sites blocked by adsorbed OH_{ad}, α and γ temperature independent transfer coefficients (= 0.5 in this case), n the number of exchanged electrons (n = 1 in this case), F the Faraday constant, c_{O2} the oxygen concentration, K a constant including all chemical parameters, and r_{OH}/RT the so called Frumkin parameter, f, describing if adsorbates behave repulsive or attractive. In the following, we will use this rate expression to analyze the effects of various factors on the kinetics of the ORR on Pt(hkl) in alkaline solution.

The experimental results presented in the previous section clearly demonstrate that in the temperature range between 293 K and 333 K the ORR in alkaline solution vary with the crystal face. There are three general observations concerning the structure sensitivity:

i) The structure sensitivity follows the potential dependent surface coverage by OH_{ad}, which in turn is determined by the relative strengths of adsorption of Pt-OH_{ad} interaction, *viz.*, (110) >(100) > (111) [18,19], with the reaction rates then varying in reverse proportion, (111) > (110) > (100). This appears to be consistent support for the proposition that the structure sensitivity of the ORR in alkaline solution mainly arises due to the structure sensitive adsorption of OH_{ad}, *i.e.*, the most active (111) surface has the lowest coverage by

OH_{ad} and weakest Pt-OH_{ad} interaction, and the least active Pt(110) surface is highly covered with more strongly adsorbed OH species. As a consequence, the structure sensitivity of the ORR on Pt(hkl) in alkaline solution is determined mainly by the $(1-\Theta_{OHad})$ term, consistent with our general proposition [8,12,14,25] that not only does structure sensitivity arise because of the sensitivity of the adsorption energy of the reactive intermediates to site geometry (see below), but also from sensitivity to site geometry of the adsorption of spectator species.

ii) A similar activation energy has been found for all three Pt(hkl) surfaces, *i.e.*, from figure 4 in the range between 37 to 47 $kJmol^{-1}$. This result may suggest that the standard free energy of adsorption of the reaction intermediates is not strongly "structure sensitive" and thus the term $r_{OH}\Theta_{OHad}$ may not play a significant role in the overall kinetics on the Pt(hkl) surfaces. As we demonstrate below, this analysis might be an oversimplification and does not necessarily capture all of the factors that contribute to the structure sensitivity of the ORR in alkaline solutions.

iii) The Tafel slope, which has a unique value for each crystal face, decreases with an increase of the temperature on all three single crystals, see Table 1. The phenomenon of deceasing Tafel slopes with increasing temperature, as summarized in Table 1, is an important new observation which is in contrast to the behavior of Pt(hkl) in solutions containing strongly adsorbing anions, viz. HSO_4^-, where the Tafel slopes were directly proportional to the temperature (from 116 $mVdec^{-1}$ at 293 K to 132 $mVdec^{-1}$ at 333 K [25]), with the transfer coefficient α being independent of temperature [25]. The latter observation is consistent with a supposition that if Pt is predominately covered by specifically adsorbing anions then the rate of the ORR in Eq. 5 is mainly determined by the $(1-\Theta_{anion})$ term [30]. If, however, a Pt electrode is covered by oxygenated species, as in a perchloric acid solution, then besides the

blocking effect, OH_{ad} can alter the adsorption energy of reaction intermediates, viz. O_2^-, HO_2^-, etc. [8,30].

To see the contribution of the $(1-\Theta_{OH})$ and $r_{OH}\Theta_{OHad}$ terms on Pt(hkl) in alkaline solution, we simulate the logi-E relationship using Eq 5 and independently determined relations for $(1-\Theta_{OHad})$ and r_{OH}. From the simulated curves we extrapolated the Tafel slopes and these values were compared with the experimentally measured Tafel slopes, see tables 1 and 2. For the $(1-\Theta_{OHad})$ term we used the experimentally determined potential dependent OH_{ad} coverage on Pt(hkl) surfaces at the respective temperature [18], which gave us the values of Θ_{OH} and the particular electrode potential, E. Therefore, with the exception of the Frumkin parameter, f=r/RT and reaction order in active sites, x, all other parameters in Eq. 5 are known (R = 8.314 J mol^{-1} K^{-1}, T = 293 to 333 K, $\alpha = \gamma = 0.5$, F = 96485 C mol^{-1}, n = 1). If f=r/RT = 0, then the adsorption of OH as well as the reaction intermediates is assumed to follow a Langmuir behavior. On the other hand, if $f=r/RT \neq 0$, the adsorption follows a Frumkin isotherm due to lateral interactions among the OH and the reaction intermediates. The Frumkin parameter f=r/RT, has been calculated previously for Pt(111) in perchloric acid solution [30]. The best fit value in that was ca. $f = 6$, implying strong lateral repulsion between OH_{ad} on the Pt(111) surface. Supposing that similar interaction may exists among OH_{ad} and reaction intermediates, we fit different values for f in eq. 5 for the two "flat" surfaces, *i.e.*, Pt(111) and Pt(100). For the more corrugated Pt(110) surface, the same model could not applied because the relationship between Θ_{OH} and the number of active Pt sites could not be established unambiguously, for details see ref. [18]. Using $x = 2$ did not lead to any agreement between the calculated and experimentally determined Tafel slopes. In order to reproduce the experimental data (Figure 5) we had to use $x = 1$ with the other parameters

summarized in Table 2. Very important features clearly emerge from Figure 5 and Table 2. First of all, the experimental Tafel slope of 86 $mVdec^{-1}$ at 293 K on Pt(111) (figure 5a) can be obtained assuming pure Langmuirian conditions. That is, the ORR at this temperature seems to be solely determined by the availability of sites for O_2 adsorption. Secondly, at 313 K and 333 K, a reasonable agreement between experimentally observed and calculated Tafel slopes can be obtained if the adsorption of reaction intermediates switches from Langmurian to Frumkin conditions at higher temperature. A further inspection of Table 2 reveals that the Frumkin parameter, *f*, increases at higher temperatures. We recall, that higher *f* values imply stronger repulsive interactions between co-adsorbed OH_{ad} and the reaction intermediates (*i.e.*, lower free energy of adsorption at given coverage), a fact which appears to be consistent with a well established change in heat of adsorption for O_2/O on Pt(hkl) in UHV [31]. Thirdly, much higher Frumkin parameters are inferred for the Pt(100) surface than for the Pt(111) surface. This observation is in agreement with the higher oxophilicity of the "open" (100) surface in comparison with the closed-packed (111) surface (see part 1 [19] and 2 [18] and the discussion of the elementary reactions at the beginning of this section).

Another point that can be clarified from the use of the kinetic model represented by Eq. 5 is the relation between temperature and the apparent transfer coefficient, α [32]. In the classical electrochemical theory for charge transfer reactions, the Tafel slope, $\partial \log i / \partial E$, is contained entirely in the $\mathbf{exp}(\alpha \boldsymbol{FE / RT})$ term, with α being a temperature-independent factor. The literature data show, however, that both the temperature dependent [33-35] as well temperature independent [25,36,37] transfer coefficients are derived from experimental data for log(i) *vs*. (αFE/RT). Conway [32] has argued that the apparent transfer coefficient is in general a temperature dependent factor having the general form $\alpha(T) = \alpha_H + \alpha_S T$, with the

indices H and S denoting its enthalpic and entropic parts, respectively. Rather than debate the interpretation here, the interested reader is referred to the original references for details. We only note that our recent analysis for the ORR on Pt(hkl) in sulfuric acid solution was consistent with the previous reports for a polycrystalline Pt electrodes that the Tafel slope is directly proportional to the temperature with the transfer coefficient α being a *temperature-independent* factor. In the case here for Pt(hkl) in alkaline electrolyte the observed decrease of the Tafel slopes with increasing temperature does not necessarily mean there is a temperature dependent transfer coefficient. We have shown that the unusual decrease of the Tafel slope with increasing temperature can be accounted for by the temperature dependence of the surface coverage of OH and the fundamental relationship connecting the reaction rate and the coverage by OH and other reaction intermediates without invoking a temperature dependent transfer coefficient. In conclusion, therefore, it appears that the ORR kinetics and the observed structural sensitivity on Pt(hkl) in alkaline solution between 293 K and 333 K is mainly determined by the coverage dependent pre-exponential term $(1-\Theta_{OH})$ and the way adsorbed OH_{ad} species and the reaction intermediates interact with each other at the Pt surface, *i.e.* the $r_{OH}\Theta_{OHad}$ term in Eq. 5.

5. Conclusion

The kinetics of the oxygen reduction reaction (ORR) was studied in alkaline electrolyte at 293-333K on Pt(hkl) surfaces by means of the rotating ring-disk electrode technique with solution phase peroxide detected at the ring electrode. The ORR on Pt(hkl) was found to be highly structure sensitive following the sequence (111) > (100) > (110)(1x2).

Very similar apparent activation energies (37 to 47 ± 5 kJmol^{-1}, η = 0.35 V) were found on all three surfaces. Furthermore, at elevated temperature, significantly smaller amounts of peroxide are formed in agreement with enhanced peroxide reduction rates by increasing temperature, which directly points to the serial reaction pathway through intermediately formed peroxide species. Based on a detailed kinetic analysis of the polarization curves and the temperature dependence of the ORR kinetics are determined by the availability of adsorption sites for the O_2 molecule, *i.e.*, the pre-exponential (1-Θ_{ad}) term, and the way adsorbed oxygenated species interact on the surface in a Frumkin-type behavior.

Acknowledgements

This work was supported by the Assistant Secretary for Conservation and Renewable Energy, Office of Transportation Technologies, Electric and Hybrid Propulsion Division of the U.S. Department of Energy under Contract No. DE-AC03-76SF00098.

	293 K [$mVdec^{-1}$] lcd/hcd[a)]	313 K [$mVdec^{-1}$] lcd/hcd [a)]	333 K [$mVdec^{-1}$] lcd/hcd [a)]	$\Delta H^{\neq}$ [$kJmol^{-1}$] [b)]
Pt(111)	--/86	--/72	--/57	47
Pt(100)	--/112	--/78	--/60	42
Pt(110)(1x2)	92/190	80/120	--/83	37

[a)] Tafel slopes determined at low (lcd) and high (hcd) current densities

b) determined at $\eta = 0.35$ V

Table 1: Summary of the experimentally determined Tafel slopes and the apparent energies of activation on Pt(hkl) in 0.1 M KOH.

Pt(111)	B [mVdec^{-1}]	Λ [mVdec^{-1}]	Φ [mVdec^{-1}]
293 K	116	84	84 *(f=0)*
313 K	124	81	68 *(f=3)*
333 K	132	87	54 *(f=9)*

Table 2a

Pt(100)	B [mVdec^{-1}]	Λ [mVdec^{-1}]	Φ [mVdec^{-1}]
293 K	116	102	--
313 K	124	110	76 *(f=12)*
333 K	132	112	65 *(f=18)*

Table 2b

Table 2: Contribution to $\partial \log i / \partial E$ from each term in Eq. 5: $\mathrm{B} = \mathbf{exp}\left(\frac{-\alpha \boldsymbol{FE}}{\boldsymbol{RT}}\right)$ (pure Butler-Volmer-term), $\Lambda = \mathbf{(1-\Theta_{OH})} \cdot \mathrm{B}$ (pure Langmuirian conditions), and $\Phi = \Lambda \cdot \mathbf{exp}\left(\frac{-\gamma \boldsymbol{r_{OH}} \Theta_{OH}}{\boldsymbol{RT}}\right)$ ($f = r_{OH}/RT$, Frumkin conditions).

References

1. A.J.Appleby, *Catal. Rev.*, 1970, **4**, 221.
2. M.R.Tarasevich, A.Sadkowski, E.Yeager, in *Comprehensive Treatise in Electrochemistry*, ed. J.O'M.Bockris, B.E.Conway, E.Yeager, S.U.M.Khan, R.E.White , Plenum Press, New York, 1983, p. 301.
3. S.Gottesfeld and T.A.Zawodzinski, in *Advances in Electrochemical Science and Engineering*, ed. R.C.Alkire, H.Gerischer, D.M.Kolb, C.W.Tobias, Wiley-VCH, Weinheim, 1997, p. 195.
4. K.Kinoshita, *Electrochemical Oxygen Technology*, John Wiley & Sons, New Vork 1992.
5. O.Haas and E.J.Cairns, *Annu. Rep. Prog. Chem. , Sect. C*, 1999, **95**, 163.
6. R.R.Adzic, N.M.Markovic, V.B.Vesovic, *J. Electroanal. Chem.*, 1984, **165**, 105.
7. F.EL Kadiri, R.Faure, R.Durand, *J. Electroanal. Chem.*, 1991, **301**, 177.
8. N.M.Markovic and P.N.Ross Jr., in *Interfacial Electrochemistry-Theory, Experiments and Applications*, ed. A.Wieckowski, Marcel Dekker Inc., New York, 1999, p. 821.
9. N.M.Markovic, T.J.Schmidt, V.Stamenkovic, P.N.Ross, *Fuel Cells*, 2001, **1**, 105.
10. V.Climent, N.M.Markovic, P.N.Ross, *J. Phys. Chem. B*, 2000, **104**, 3116.
11. U.A.Paulus, A.Wokaun, G.G.Scherer, T.J.Schmidt, V.Stamenkovic, N.M.Markovic, P.N.Ross Jr., *J. Phys. Chem. B*, 2002, **106**, 4181.
12. T.J.Schmidt, V.Stamenkovic, M.Arenz, N.M.Markovic, P.N.Ross Jr., *Electrochim. Acta*, 2002, in press.
13. N.M.Markovic, H.A.Gasteiger, P.N.Ross, *J. Phys. Chem.*, 1995, **99**, 3411.
14. N.M.Markovic, H.A.Gasteiger, P.N.Ross, *J. Phys. Chem.*, 1996, **100**, 6715.
15. A.J.Appleby, in *Comprehensive Treatise in Electrochemistry*, ed. B.E.Conway, J.O'M.Bockris, S.U.M.Khan, R.E.White , Plenum Press, New York, 1983, p. 173.

16. R.R.Adzic, in *Electrocatalysis* , ed. J.Lipkowski, P.N.Ross, Wiley-VCH, Inc., New York, 1998, p. 197.

17. N.M.Markovic, T.J.Schmidt, B.N.Grgur, H.A.Gasteiger, P.N.Ross Jr., R.J.Behm, *J. Phys. Chem. B*, 1999, **103**, 8568.

18. T.J.Schmidt, N.M.Markovic, P.N.Ross Jr., *J. Phys. Chem. B*, 2001, **105**, 12082.

19. T.J.Schmidt, N.M.Markovic, P.N.Ross Jr., *J. Electroanal. Chem.*, 2001, **524-525**, 252.

20. N.M.Markovic, B.N.Grgur, C.A.Lucas, P.N.Ross, *Surf. Sci.*, 1997, **384**, L805.

21. F.T.Wagner and P.N.Ross Jr., *J. Electroanal. Chem.*, 1988, **250**, 301.

22. T.J.Schmidt, U.A.Paulus, H.A.Gasteiger, N.Alonso-Vante, R.J.Behm, *J. Electrochem. Soc.*, 2000, **147**, 2620.

23. U.A.Paulus, T.J.Schmidt, H.A.Gasteiger, R.J.Behm, *J. Electroanal. Chem.*, 2001, **495**, 134.

24. A.Parthasarathy, S.Srinivasan, A.J.Appleby, C.R.Martin, *J. Electrochem. Soc.*, 1992, **139**, 2530.

25. B.N.Grgur, N.M.Markovic, P.N.Ross Jr., *Can. J. Chem.*, 1997, **75**, 1465.

26. N.A.Anastasijevic, V.B.Vesovic, R.R.Adzic, *J. Electroanal. Chem.*, 1987, **229**, 305.

27. V.S.Bagotzky, M.R.Tarasevich, V.Y.Filinovskij, *Élektrokhimiya*, 1969, **5**, 1218.

28. H.S.Wroblowa, Y.Pan, G.Razumney, *J. Electroanal. Chem.*, 1976, **69**, 195.

29. R.A.Sidik and A.B.Anderson, *J. Electroanal. Chem.*, 2002, **528**, 69.

30. N.M.Markovic, H.A.Gasteiger, B.N.Grgur, P.N.Ross, *J. Electroanal. Chem.*, 1999, **467**, 157.

31. R.I.Masel, *Principles of Adsorption and Reaction on Solid Surfaces*, John Wiley & Sons, New York 1996.

32. B.E.Conway, in *Modern Aspects of Electrochemistry*, ed. B.E.Conway, J.O'M. Bockris, R.E.White, Plenum Press, New York, 1986, p. 103.

33. B.R.Scharifker, P.Zelenay, J.O'M. Bockris, *J. Electrochem. Soc.*, 1987, **134**, 2714.

34. M.A.Enayetullah, T.D.DeVilbiss, J.O'M. Bockris, *J. Electrochem. Soc.*, 1989, **136**, 3369.

35. A.Damjanovic and D.B.Sepa, *Electrochim. Acta*, 1990, **35**, 1157.

36. A.J.Appleby, *J. Electrochem. Soc.*, 1970, **117**, 328.

37. A.J.Appleby, *J. Electrochem. Soc.*, 1970, **117**, 641.

Figure Captions

Figure 1: **(a)** Base voltammetry of Pt(111) (50 mVs^{-1})at 293 K (solid line) and 333 K (dashed line). **(b)** Family ORR polarization curves (50 mVs^{-1}, anodic sweeps) at different rotation rates at 333 K on Pt(111). **(c)** Molar fraction of peroxide formation during the ORR at 293 K, 313 K, and 333 K, respectively. **(d)** Tafel plots for Pt(111) deduced from the polarization curves at 2500 rpm at 293 K, 313 K, and 333 K, respectively.

Figure 2: **(a)** Base voltammetry of Pt(100) (50 mVs^{-1})at 293 K (solid line) and 333 K (dashed line). **(b)** Family ORR polarization curves (50 mVs^{-1}, anodic sweeps) at different rotation rates at 333 K on Pt(100). **(c)** Molar fraction of peroxide formation during the ORR at 293 K, 313 K, and 333 K, respectively. **(d)** Tafel plots for Pt(100) deduced from the polarization curves at 2500 rpm at 293 K, 313 K, and 333 K, respectively.

Figure 3: **(a)** Base voltammetry of Pt(110) (50 mVs^{-1})at 293 K (solid line) and 333 K (dashed line). **(b)** Family ORR polarization curves (50 mVs^{-1}, anodic sweeps) at different rotation rates at 333 K on Pt(110). **(c)** Molar fraction of peroxide formation during the ORR at 293 K, 313 K, and 333 K, respectively. **(d)** Tafel plots for Pt(110) deduced from the polarization curves at 2500 rpm at 293 K, 313 K, and 333 K, respectively.

Figure 4: Arrhenius plots at $\eta = 0.35$ V for the ORR between 293 K and 333 K on Pt(hkl)

Figure 5: Fitted (simulated) Tafel plots on **(a)** Pt(111) and **(b)** Pt(100) as described in the text using the experimentally determined OH_{ad} adsorption isotherms [18]

Figure 6: (a) ORR Polarization curves from potentiodynamic (50 mVs^{-1}, solid line) and potentiostatic (gray circles) measurements (1600 rpm) at 293 K along with the base CV (50 mVs^{-1}, dashed line). **(b)** ORR Polarization curves from potentiodynamic (50 mVs^{-1}, solid and dashed lines represent the anodic and cathodic sweep, repsectively) and potentiostatic (gray circles) measurements (1600 rpm) at 333 K. Potential was held for 5 minutes before recording the potentiostatic currents.

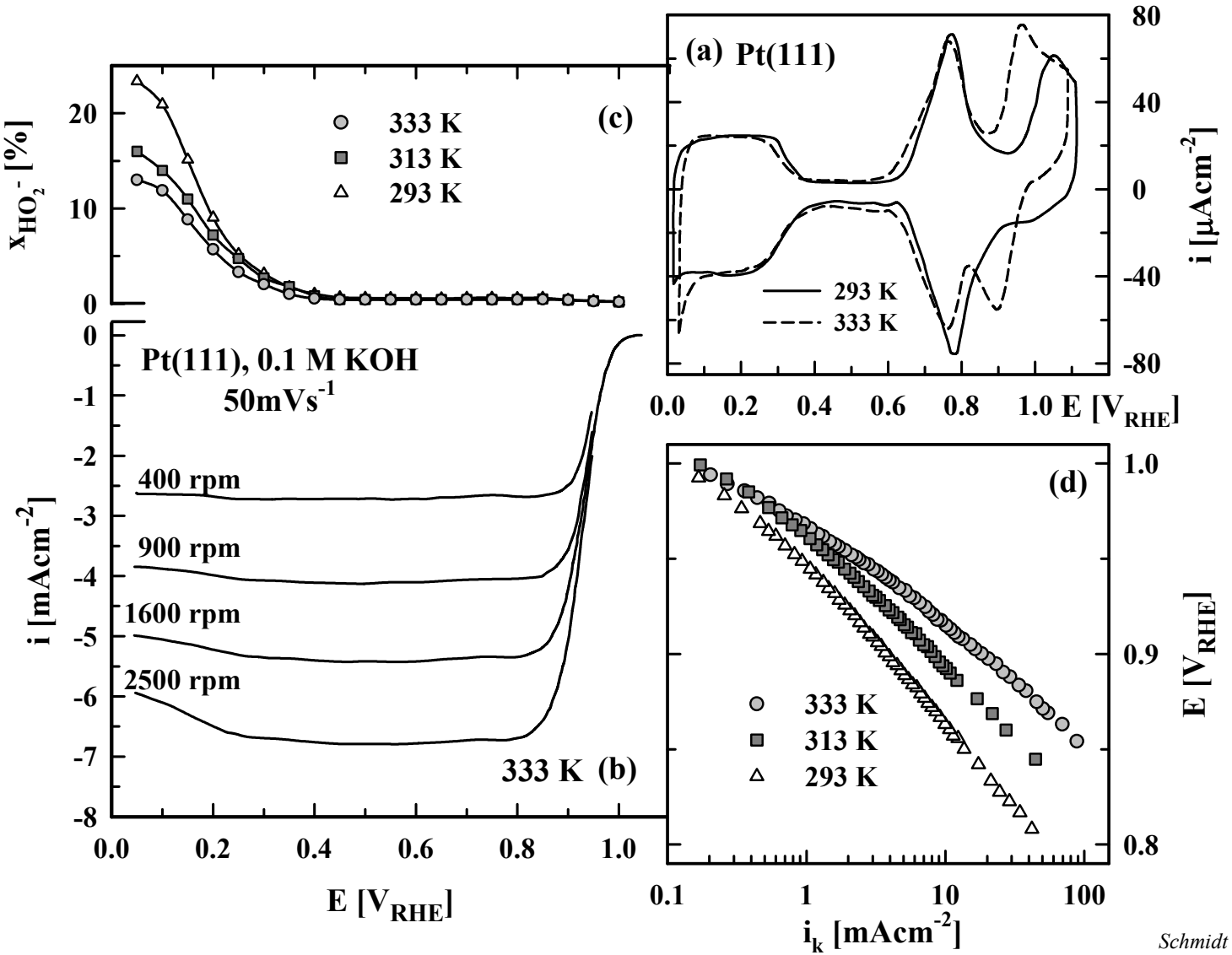

Schmidt et al., figure 1

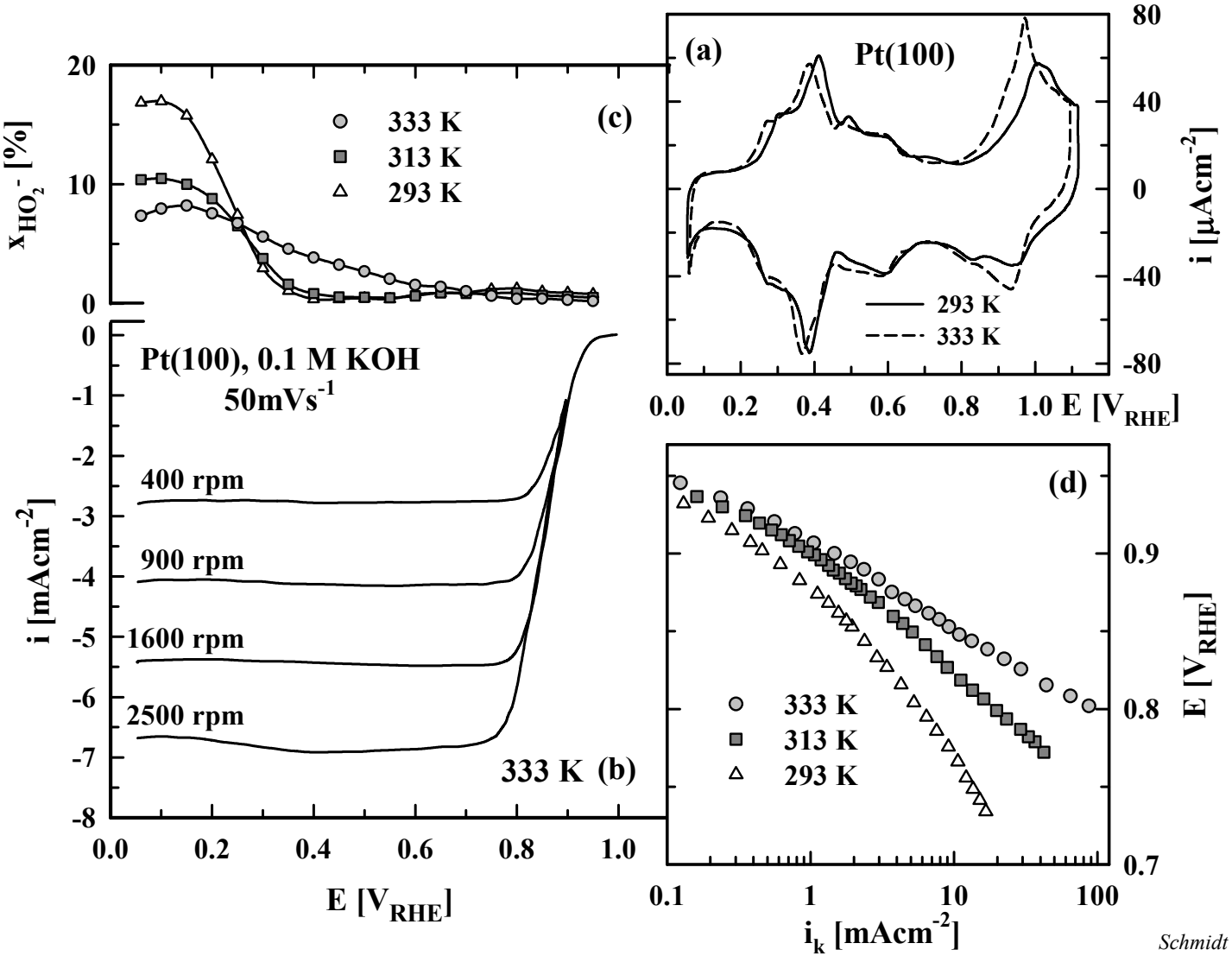

Schmidt et al., figure 2

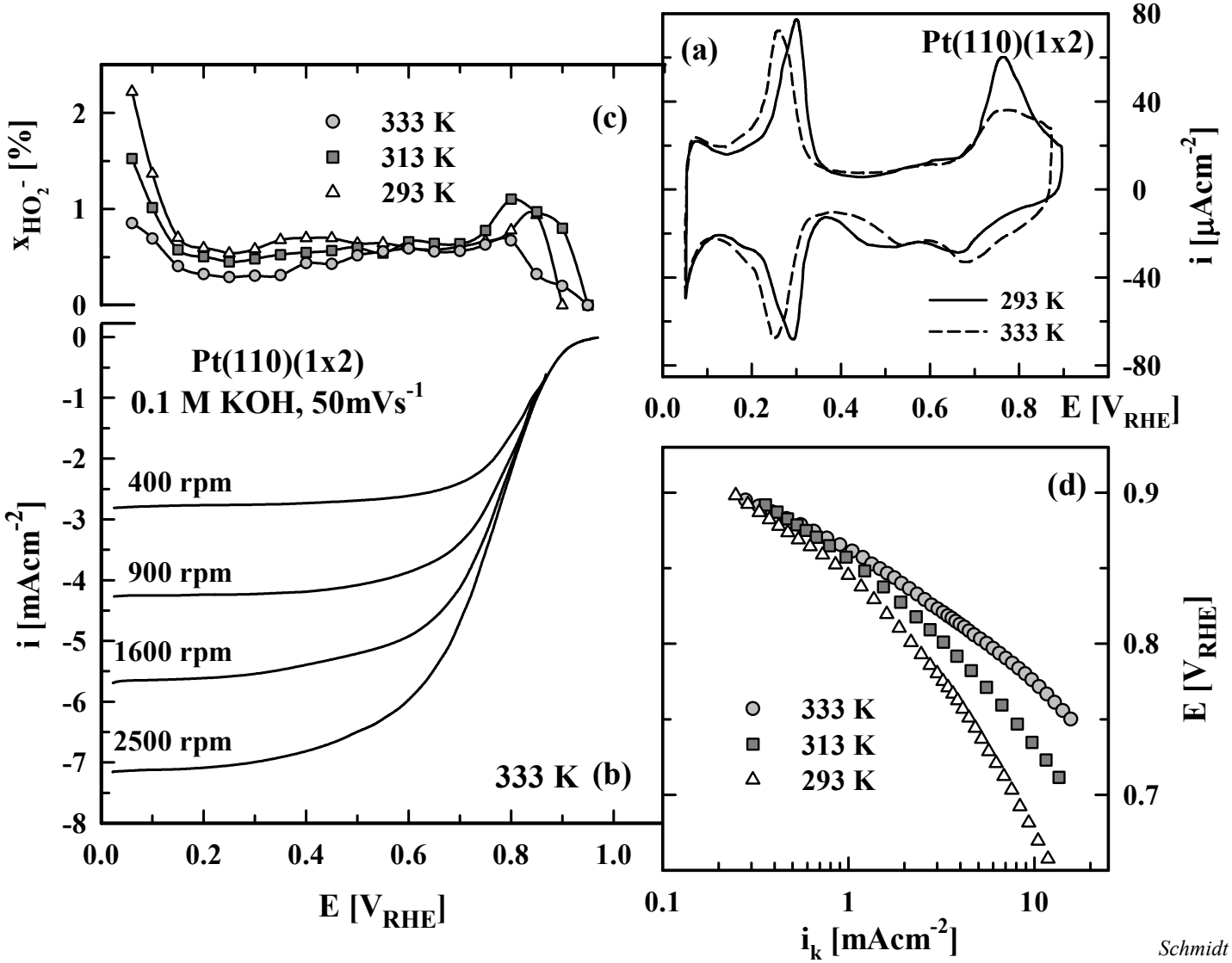

Schmidt et al., figure 3

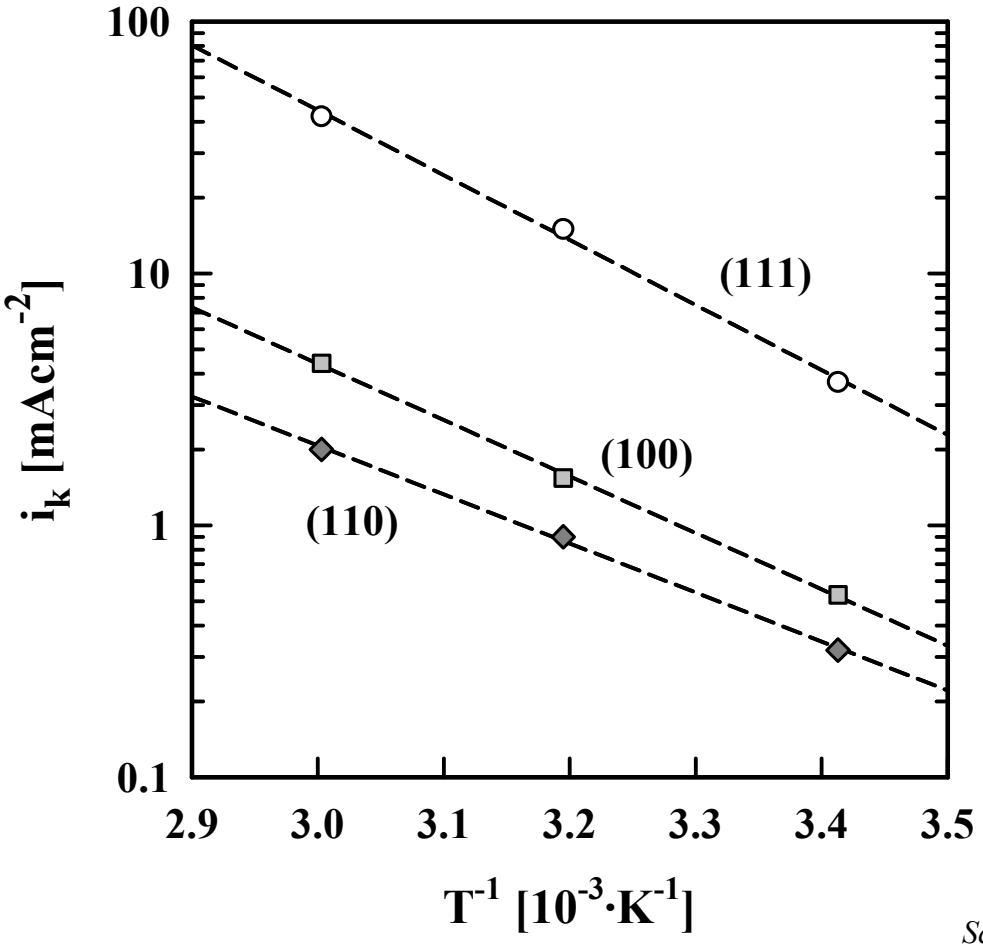

Schmidt et al., figure 4

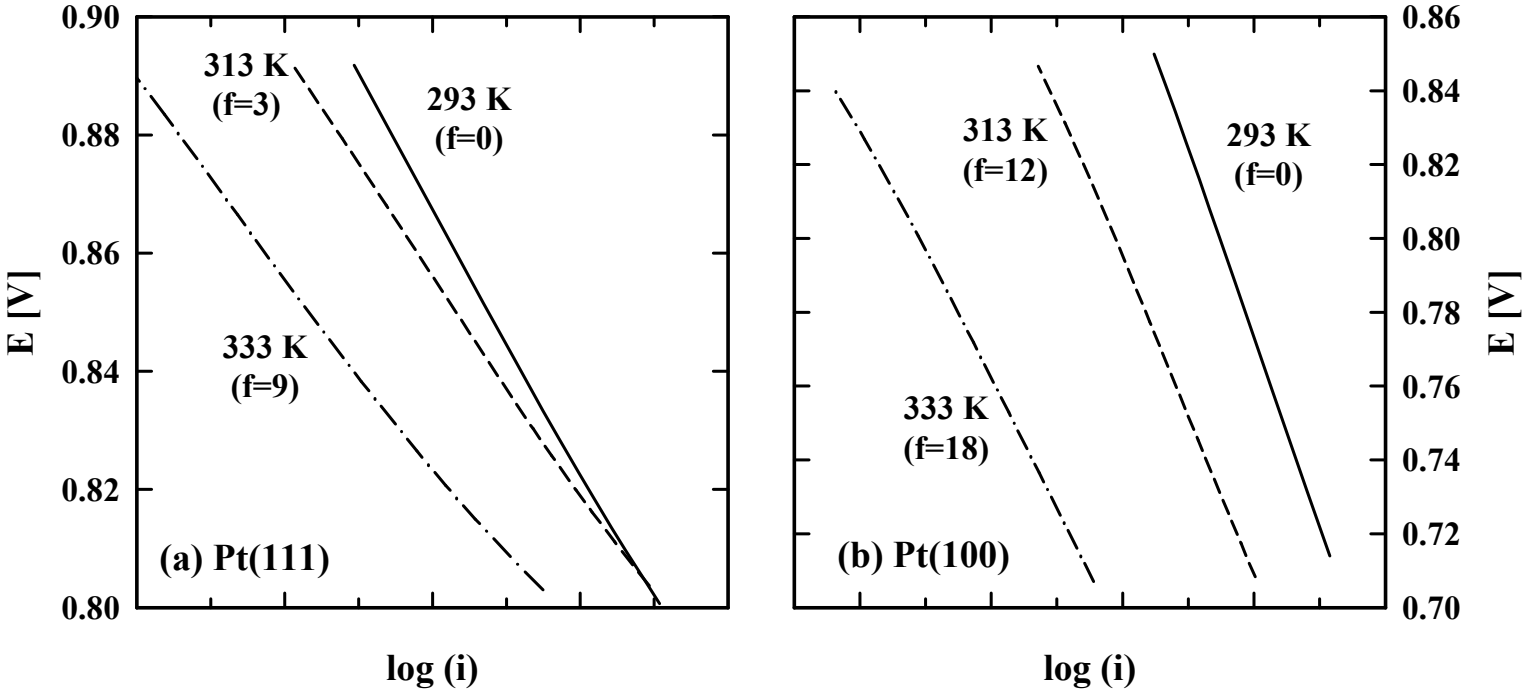

Schmidt et al., figure 5

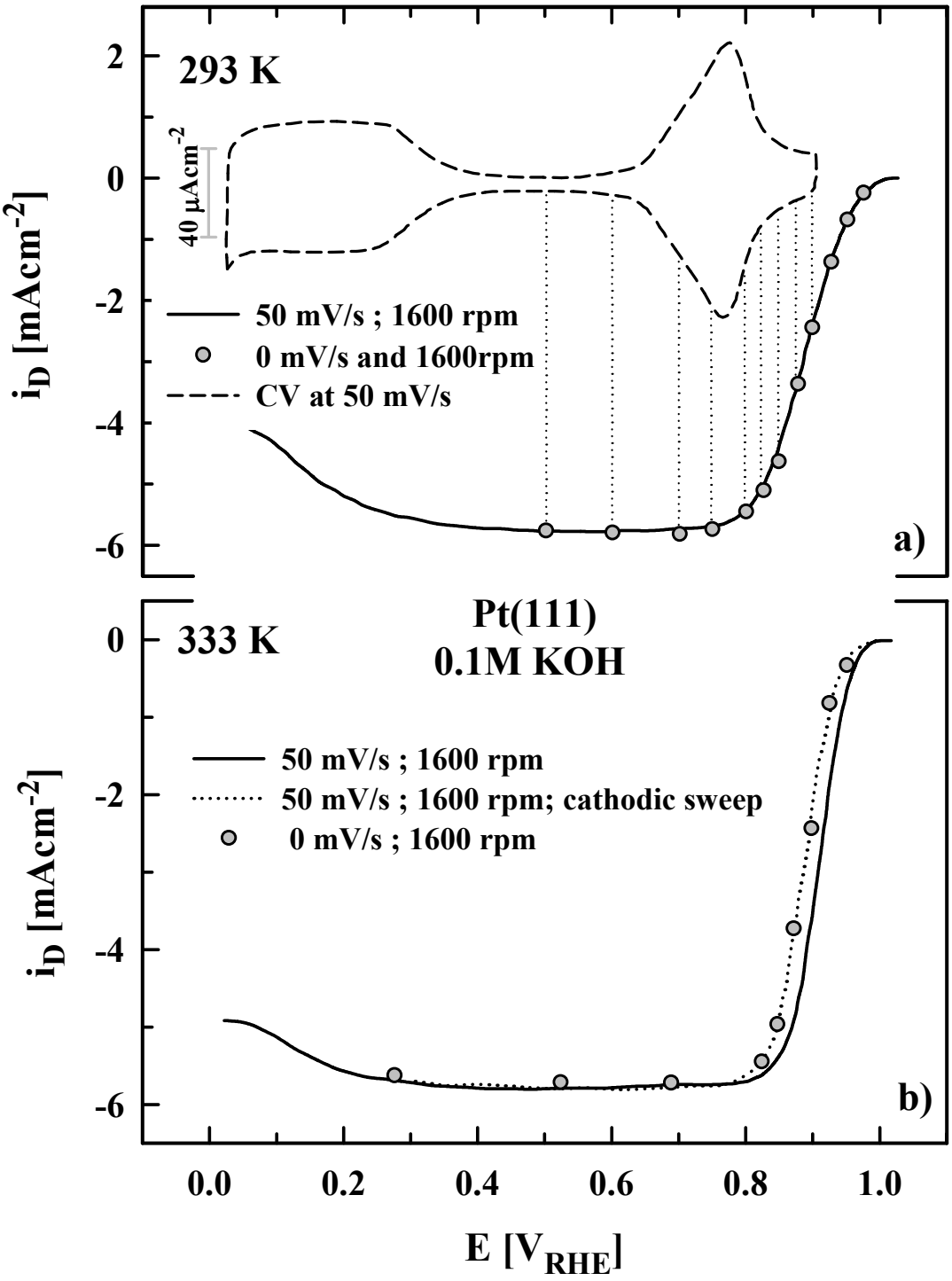

Schmidt et al., figure 6